The consistency evaluation of the climate version of the Eta regional forecast model developed for regional climate downscaling.

I. A. Pisnichenko* T.A. Tarasova*

20 May 2007

Abstract

The regional climate model prepared from Eta WS (workstation) forecast model has been integrated over South America with the horizontal resolution of 40 km for the period of 1961-1977. The model was forced at its lateral boundaries by the outputs of HadAMP. The data of HadAMP represent the simulation of modern climate with the resolution about150 km.

In order to prepare climate regional model from the Eta forecast model was added new blocks and multiple modifications and corrections was made in the original model.

The running of climate Eta model was made on the supercomputer SX-6. The detailed analysis of the results of dynamical downscaling experiment includes an investigation of a consistency between the regional and AGCM models as well as of ability of the regional model to resolve important features of climate fields on the finer scale than that resolved by AGCM.

*Centro de Previsão de Tempo e Estudos Climáticos/Instituto Nacional de Pesquisas Espaciais, Cachoeira Paulista, SP, Brazil, (pisnitch@cptec.inpe.br). On leave from A.M. Obukhov Institute of Atmospheric Physics, Russian Academy of Sciences, Moscow, Russia.

In this work we show the results of our investigation of the consistency of the output fields of the Eta model and HadAMP. We have analysed geopotential, temperature and wind fields. For the evaluation of the likeness of these two models output we used Fourier analysis of time series, similarity index, constituted from linear regression coefficients, time mean and space mean bias, square error, dispersion analysis and some others characteristics. This investigation demonstrates that the regional model characteristics do not have any positive or negative significant trend in relation to the global model data. From the total analysis we can affirm that in the description of climate behaviour these two models are in consistency.

1. Introduction

The time averaged large-scale meteorological fields (>500 km) are actively studied in the works on climate theory and climate change analysis. Needs of agriculture, industrial and energy development planning require the knowledge of detailed, regional and local scale (100km - 10 km) climatic information. As the modern net of climate observation stations can supply data only suited for large-scale climate field investigations, the dynamical downscaling using high-resolution regional climate model (RCM) is the most powerful instrument for obtaining the smaller-scaled climate information. For the study of regional climate change in the future the dynamical downscaling is the only way to obtain necessary information. The dynamical downscaling approach involves RCM forced at the lateral and bottom boundaries by an atmospheric general circulation model (AGCM) or reanalysis data (e.g. Dickinson et al. 1989). The finer regional-scale features of RCM can be attributed to detailed topography and land surface features, more comprehensive parameterization of unresolved physical processes in the model equations, and explicit simulation of large mesoscale processes.

Atmosphere-ocean general circulation models (AOGCM) with the horizontal resolution of a few hundred kilometers are currently used for the simulation of large-scale response of the climate system to increasing of greenhouse gases and aerosol concentrations in the future. The running of RCM with the horizontal resolution of a few tens of kilometers over an area of interest with the boundary conditions of AOGCM for the periods of 10-30 years in the present and in the future can give additional information about the regional-scale climate and climate-change effects in this area. Such climate-change simulations with RCM have been made already for various parts of Europe, North America, Australia, and Africa; see for example the references cited by Jones et al. (1997); Laprise et al. (2003); Giorgi et al. (2004); Duffy et al. (2006). Currently some large projects (PRUDENCE (Christensen et al., 2002) and NARCCAP (http://www.narccap.ucar.edu)) launched to investigate uncertainties in the RCM climate-change simulations over Europe and North America are underway. The project "Climate change scenarios using PRECIS" (Jones et al. 2004) was launched by Hadley Center for Climate Prediction and Research to develop user-friendly RCM which can be easily running on personal computer for any area of the globe. The South American countries including Brazil are participated in this project running PRECIS over various parts of South America. The data of the atmospheric global model HadAM3P were provided by Hadley Center for using them as boundary conditions in these simulations.

The published studies of downscaling over South America are relatively few as compared with those made over other continents. Most of them are limited to continuous integration periods of 1-5 months during 1-5 years with different RCMs (Nobre et al. 2002; Roads et al. 2003; Misra et al. 2003; Sun et al. 2005). The NCEP Eta Model (Mesinger et al. 1988) was intensively used for the weather forecast and climate studies over South America during last decade (Tanajura, 1996; Chou et al., 2000; Chou et al. 2002; Tarasova et al. 2006; Gonsalves et al., 2006). The impact of the Andean topography, different land surface schemes, radiation schemes, convection schemes, and initial soil moisture fields on the model performance, was studied. Analysis of the integration results demonstrates in some cases a significant improvement of climate information as compared with AGCM. It was shown that after downscaling the surface temperature and precipitation in the interior of the continent during wet months became more close to observation data, the high-frequency precipitation statistics in the north-east part of Brazil were improved, some AGCM biases relatively observations were corrected. Nevertheless, the longest integrations with the Eta model were limited to the continuous integrations for 3-5 months. This is related to the limitations in the codes of the Eta model which was developed for forecast studies. Nevertheless the Eta model can be used for climate integrations because it has efficient and scalable code and considers the long-term balances (Mesinger et al., 1988). The climate versions of the Eta model which allow integrations longer than 5 months were developing at the Brazilian Instituto Nacional de Pesquisas Espaciais/Centro de Previsao de Tempo e Estudos Cimaticos (INPE/CPTEC) during last years (Pisnichenko et al. 2006; Fernandez et al. 2006; Tarasova et al. 2006).

In this paper we present the new version of the Eta model which we developed for the climate-change simulations. The short description of the Eta model and of the modifications which we implemented is given in Section 2. In this section it is also described the model integration procedure. The newly developed version of the Eta model is hereafter termed as INPE Eta for Climate Change Simulations (INPE Eta CCS). Section 3 presents the results of the integrations with the INPE Eta CCS model over South America driven by boundary conditions from the HadAM3P for the period 1961-1991. Its output fields are compared with those from HadAM3P in order to prove a consistency between the two models. Section 4 gives summary of the results and conclusions.

2. Model and experimental design

For this work, aimed to prepare Eta model version for climate-change simulations, we initially adopted the workstation (WS) Eta modeling package (version of 2003) developed at the Science Operations Officer/Science and Training Resource Center (SOO/STRC). This package and its User Guide written by R. Rozumalski is freely available at http://strc.comet.ucar. The SOO/STRC WS Eta is nearly identical to WS Eta model and operational Eta Model of 2003 both developed at NCEP. Only the run-time scripts and model files organization were changed. The additional convection cumulus scheme of Kain and Fritsch (1993) was also implemented. The longest continuous integration with this model can be made for 1 month due to the restriction on the output file name, restart subroutines, and some other impediments.

a. Short description of NCEP Eta model

The full description of the NCEP Eta regional forecasting model is given by Mesinger et al. (1988); Janjic (1994); and Black (1994). In short, the horizontal field structure is described on a semi-staggered E grid. The eta vertical coordinate is used to reduce numerical errors over mountains in computing the pressure gradient force (Mesinger et al., 1988). The planetary boundary layer processes are described by the Mellor-Yamada level 2.5 model (Mellor and Yamada, 1974). The convective precipitation scheme is of Betts and Miller (1986) modified by Janjic(1994). The shortwave and longwave radiation codes follow parameterizations of Lacis and Hansen (1974) and Fels and Schwartzkopf (1975), respectively. The land-surface scheme is of Chen et al. (1997). The grid-scale cloud cover fraction is parameterized as a function of relative humidity and cloud water (ice) mixing ratio (Xu and Randall, 1996; Hong et al., 1998). Convective cloud cover fraction is parameterized as a function of precipitation rate (Slingo, 1987).

b. Modifications in the SOO/STRC WS Eta model

The SOO/STRC WS Eta model has been installed at supercomputer NEC SX6 at CPTEC. To be able to perform long term climate integrations we have made multiple changes and corrections in the scripts and source codes of the original model as well as developed the new programs.

As it was already mentioned, the Eta model was forced at its lateral and bottom boundary by the output of HadAM3P model. The HadAM3P output data represent horizontal wind, potential temperature, specific humidity and earth surface pressure which are given on the horizontal Arakawa B-grid and at 19 sigma-hybrid levels. These data are written in PP-format. To use them for the Eta model boundary conditions these data have to be transformed into horizontal wind, geopotential, mixture ratio and earth surface pressure given on regular latitude-longitude grid at standard p-surface levels. For this aim, some of the pre-processing Eta model programs were modified and new program which converts the HadAM3P output data to those acceptable by the Eta model was written.

Another modifications made in the Eta model can be shortly described as following. There were re-written the SST update programs used to accept the SST and SICE data generated by HadCM3 every 15 days. The programs of the Sun's elevation angle and of calendar were modified in order to be able to integrate the Eta model for the artificial year of 360 days which is used by HadAM3P. There were developed new restart programs which can be used in multiprocessing integration. These programs allow to continue the model integration from any time moment by using the model output binary files. This is the useful option for long term climate integration because of the large size of the file of boundary conditions needed for continuous integrations. Another reason for use of the restart option is the large size of the output binary files which after post-processing can be written in more economic GRIB format. All shortcomings which restrict a period of model integration were corrected including those in the post-processing subroutines.

The additional solar radiation scheme (CLIRAD-SW-M) developed by Chou and Suarez (1999) and modified by Tarasova and Fomin (2000) was implemented in the model. The results of the month integration with this scheme were analyzed by Tarasova et al. (2006). The additional thermal radiation scheme of Chou et al. (2001) was also implemented. This allows to run the model with increasing concentration of CO_2 and other trace gases needed for future climate simulation experiments. All these corrections, modifications and implementations were made taking into account that the model can be run on Linux cluster or any other multi-processors computer.

c. Integration with the INPE Eta CCS model

The first step in evaluation of dynamical downscaling results is investigation of a consistency between regional model outputs and GCM data used for RCM boundary conditions. That is, we have to show that our RCM does not significantly diverge from GSM in reproducing time mean large scale patterns of circulation. We also expect that both models reproduce a low-frequency oscillation of the atmosphere in a similar manner.

For this aim we analyzed the results of the Eta CCS model integration for the period 1960-1990 over South America. These data are the part of the results of current and future climate downscaling experiments covering the periods of 1960-1990 and 2071-2100, respectively. The detailed analysis of the results of these experiments is currently making by our group and will be present in further publications.

The Eta CCS model in our experiments was forced at its lateral and bottom boundary by the output of HadAM3P, which was run using SST, SICE (sea ice) and greenhouse gases and aerosol concentration as external driving from coupling model HadCM3. Data for lateral boundary conditions for the Eta CCS model were provided every 6 hours and SST and SICE data every 15 days. Linear interpolation for values on lateral boundaries, SST, and SICE was used between these periods. For the initial conditions of soil moisture and soil temperature the climate mean values were used. The spin up period of soil moisture and temperature we have accepted to be about of 1 year. Hence, the first year of the integration was not used in analysis.

Area of the integration was centered at $58.5°$ W longitude and $22.0°$ S latitude and cover the territory of South American continent with adjacent oceans ($55°$ S - $16°$ N, $89°$ W - $29°$ W). The model was integrated on 211×115 horizontal grid with grid spacing of 37 km. In the vertical, 38 eta coordinate layers were used. For modern climate integration the Betts-Miller cumulus convection parametrization scheme and the ETA model original shortwave and longwave radiation schemes were chosen.

3. Analysis of the integration results

The verification of a consistency between the outputs of the Eta CCS model and HadAM3P is particularly important due to the difference between the physical parameterization packages of these two models. To prove an agreement between these models results we have compared the geopotential height, temperature and kinetic energy fields on the earth surface and at the various p-levels (1000 mb, 700 mb, 500 mb) from these two data sources. More detailed comparison was made for the five regions shown in Figure 1: Amasonia ($12.5°$ S - $5°$ N, $75°$ W - $48.75°$ W); Nordeste (north-east of Brazil) ($15°$ S - $2.5°$ S, $45°$ W - $33.75°$ W); South of Brazil ($32.5°$ S - $22.5°$ S, $60°$ W - $48.75°$ W); Minas ($22.5°$ S - $15°$ S, $48.75°$ W - $41.25°$ W); Pantanal ($17.5°$ S - $12.5°$ S, $60°$ W - $52.5°$ W). The time averaged fields and time series of space averaged meteorological variables were analyzed.

a. Methods of the analysis

A number of measures of consistency between the outputs of the Eta CCS regional model (hereafter RM) and HadAM3P global model (hereafter GM) are used here. The original package of programs was developed for comparing the models. First, we assessed the climatological means and biases, which give an opportunity to identify systematic difference between the models. Then we analyzed various characteristics which allow to study in detail the difference between the model-simulated fields. For this comparison the regional model fields were scaled to the global model grid. For this aim we removed the small scale component from the regional model fields applying smoothed filter. This filter is the two dimensional version of the weighted moving averages, where the weights depend linearly on the distance between the grid points of global and regional models. The weight increases when the distance decreases. This can be written as:

$$\Phi(x_i, y_j) = \sum_{r_{i,j;k} < r_0} \phi(x_k, y_k)\, p_k \qquad (1)$$

where $\Phi(x_i, y_j)$ is a smoothed value of regional model field on global grid point, r_0 radius of influence which defines the circle inside which the RM field data are used for average calculation, $r_{i,j;k}$ - the distance from a (x_i, y_j) point to RM grid point k, $\phi(x_k, y_k)$ are the field value at RM grid point k inside the circle, p_k is a weight for the field value at point k which is calculated as

$$p_k \;=\; \left(1 - \frac{r_{i,j;k}}{r_0}\right) \Big/ \left(\sum_{r_{i,j;k} < r_0} 1 - \frac{1}{r_0} \sum_{r_{i,j;k} < r_0} r_{i,j;k}\right). \qquad (2)$$

In order to compare the models we analyzed how they reproduce the time average fields of meteorological variables as well as the fields of dispersion of these variables. For more detailed assessment of the consistency between the RM and GM fields we also calculated the bias and coefficients of linear regression using time-series of meteorological variables at each grid point of the Eta model. The fields of these characteristics present useful information about a degree of consistency of the models results.

For the calculation of averages, dispersions, and coefficients of linear regression by using the model output data we used the following recursive formulas:

a) for average

$$\bar{x}_n = \frac{n-1}{n}\bar{x}_{n-1} + \frac{1}{n}x_n \tag{3}$$

b) for dispersion

$$D_n = \frac{n-1}{n}D_{n-1} + \frac{n-1}{n^2}(\bar{x}_{n-1} - x_n)^2 \tag{4}$$

c) for covariance

$$r_n = \frac{n-1}{n}r_{n-1} + \frac{n-1}{n^2}(\bar{x}_{n-1} - x_n)(\bar{y}_{n-1} - y_n), \tag{5}$$

where $\bar{x}_n$, D_n, r_n are an average, a dispersion, and a covariance correspondingly for series consisting from n numbers, $\bar{x}_{n-1}$, D_{n-1}, r_{n-1} the same for series consisting from $n-1$ numbers, x_n, y_n are n-th number of series.

b. Assessment of the RM and GM consistency

At first we present geopotential height, temperature and kinetic energy fields averaged over the period of integration from 1960 to 1990. Figures 2 and 3 show these fields at the levels of 1000 mb and 700 mb, respectively, obtained from the RM and GM integrations. A comparison of both models fields at the 1000 mb level shows good agreement between the fields of geopotential height and between the temperature fields. There is general agreement between the kinetic energy fields. Some disagreement in the temperature magnitude exists in the central part of tropical South America. The values of kinetic energy differ over most part of the continent. This is probably related to the different physical parameterization packages in these models. The same RM and GM fields at the higher level of 700 mb bear closer spatial and quantitative resemblance. Note, that the fields similarity at 500 mb (not shown) is higher than that at 700 mb. This is a consequence of the diminishing of the impact of surface-atmosphere interaction on the higher-level atmospheric circulation. We also compared the same RM and GM fields averaged over January and July (not shown). The agreement between the fields is better in July (austral winter) than in January (austral summer). The fields of time dispersion of meteorological variables provide additional information about an amplitude of their temporal fluctuations. Figure 4 presents the RM and GM dispersion fields of geopotential height, temperature and kinetic energy at the 1000 mb level averaged over the period of integration. One can see reasonably high degree of consistency between the RM and GM dispersion fields. The dispersion fields also bear closer resemblance for geopotential height and temperature than for kinetic energy. With the increase of altitude the difference between the RM and GM dispersion fields is diminished for all variables.

The quantitative difference between the two fields is usually described by the fields of bias. The left column of Figure 5 shows the bias between the RM and GM geopotential height, temperature, and kinetic energy fields at 1000 mb averaged over the period of integration. One can see that the largest bias is seen over the tropical and sub-tropical parts of the Southern American continent. The significant values of the bias over the Andes is probably related to the errors of interpolation from the sigma-hybrid surfaces to the pressure surfaces located below the Earth's surface in the global model. With increasing of the altitude (700 mb, 500 mb) the values of bias decrease for all fields (not shown). The bias of these variables averaged over July (January) is smaller (larger) than that averaged over all period of integration.

For quantitative description of the consistency between the RM and GM outputs fields we propose to use a new characteristics which we termed a consistency index (CI). In order to get the numeric value of this characteristics we firstly calculated coefficients of linear regression (a1, a0) of GM time series on RM time series for each grid point of a considered field. We define CI as equal to 1 minus a ratio of two areas shown in Figure 6. The numerator of the ratio is the area of the figure formed by ideal linear regression line (a1=1.0, a0=0.0), real linear regression line (a1, a0) and by two verticals that intersect these regression lines. The abscissas of the verticals are $a - s$ and $a + s$, where a is mean value of RM time series and s is mean value of semi-width of gaussian curve calculated from the dispersion of RM time series. The denominator is the value of the area of the figure formed by ideal linear regression line (a1=1.0, a0=0.0), the regression line (a1=0, a0=$a - s$ (or a0=$a + s$)), and the verticals with the abscissas of $a - s$ and $a + s$. The horizontal regression line corresponds to the case when the RM and GM time series are non-correlated and mean value of GM time series is equal to $a - s$ (or $a + s$). The right column of Figure 5 presents the CI fields of geopotential height, temperature, and kinetic energy at the level of 1000 mb. The magnitude of CI which is close to 1 means good resemblance between the RM and GM fields. The CI fields resemble the fields of bias in terms of spatial distribution. But the use of non-dimensional characteristics CI in spite of bias allows to compare quantitatively a similarity of the fields of different meteorological variables. Thus, the CI fields in Figure 5 show that the consistency of the fields of geopotential height is higher than that of the temperature fields and the consistency of the kinetic energy field is lower than that of both geopotential height and temperature.

To compare the model outputs we also analyzed a temporal variations of the geopotential height, temperature and kinetic energy values at 1000 mb and 500 mb levels, averaged over all integration domain and over the regions shown in Figure 1. Figure 7 presents monthly mean bias and root mean square errors (RMSE) between the GM and RM time series for these variables averaged over the integration domain. For each variable the upper figure represents bias and the lower figure shows RMSE. One can see that the magnitude of mean bias is not high. It is about 6 m in geopotential height, less than 0.1 $^{\circ}$K in temperature, and about 10 m^2 sec^{-2} in kinetic energy at 1000 mb. The mean RMSE values at 1000 mb are not high also. Its magnitude is about 24 m in geopotential heights, 3.4 $^{\circ}$K in temperature, and 39 m^2 sec^{-2} in kinetic energy. Low magnitude of RMSE proves that current absolute values of bias are not high for each moment of integration. Figure 7 shows also that there is no drift of bias and RMSE during the integration that proves RM integration stability. The magnitude of temporal correlation coefficient between the time series of RM and GM space averaged fields is about 0.95-0.98. This means that RM follows the GM boundary driving. At the level of 500 mb as bias as RMSE are of lower or same magnitude. We also analyzed the same time series for the above mentioned regions (Amasonia, Nordeste, South of Brazil, Minas, Pantanal). The correlation coefficients between the RM and GM time series as well as mean biases and RMSE at 1000 mb and 500 mb are shown in Table 1 for all domain and for the five regions. One can see that these coefficients slightly varies from region to region. Note one case of low correlation between the kinetic energy time series at 1000 mb in Amazonia related to low magnitude of wind at the surface level in GM.

Figures 8 and 9 show the time evolution of annual mean bias in the geopotential height, temperature and kinetic energy fields at 1000 mb and 700 mb, respectively, for the above mentioned regions. At the 1000 mb level the magnitude of bias for different regions varies from -10 m to +17 m for geopotential height, from -4.0°K to +0.3°K for temperature, and from -20 $m^2\,sec^{-1}$ to -5 $m^2\,sec^{-1}$ for kinetic energy. The amplitude of interannual variations of these meteorological variables differs from one region to another. We can see that there is no significant trend and strong fluctuations of bias for any region. A significant mutual correlation between the biases for various regions does not exist. Note that the values of bias and the amplitudes of its interannual variations for geopotential height and temperature decrease when the altitude increases. For kinetic energy both bias and amplitude of interannual variations increase when the altitude increases. Though the magnitude of relative bias (for example, that divided by a mean dispersion) for kinetic energy also decreases.

Figure 10 presents a scattering diagram of daily linear regression coefficients values (a0, a1) which describe the regression of the GM 1000 mb geopotential height field on the same

RM field (top); time evolution of these linear regression coefficients (a0 , a1) (middle) for each month of the model run; and the time evolution of consistency index (bottom). The consistency index was calculated in the same way as described above (Figure 6), but the time series were substituted by "space" series formed by variable values at all grid points.

Concerning this figure we can say that in the hypothetical case, when the fields of GM and RM coincide, all points in the top figure will fall on one point with the coordinates a1=1.0 and a0=0.0. Thus we can affirm that if the points on the top figure are located near the point (a1=1, a0=0) the RM and GM fields are very similar; in the case when the points are reasonably scattered but the center of mass of this distribution is close to the point (a1=1, a0=0) we can say that the fields of the models are similar in average. The time series of linear regression coefficients a0 and a1 of GM data upon RM data have large negative correlation (middle figure). In the most cases it leads to some compensation in the variations of CI shown on the bottom figure. The CI variations clearly express the year oscillation. Its mean value is about 0.94 and increases with the altitude. Its linear time trend is very small. This provides some more indication that the considered models do not diverge. Figure 11 presents the same characteristics as shown in Figure 10 but for the RM and GM temperature fields at 1000 mb. The scattering diagrams in this case indicates that GM is slightly warmer then RM for the regions with low temperatures and slightly colder for the regions with higher temperatures. This is in agreement with Figure 2 which shows mean temperature fields for all period of the integration.

For more detailed analysis of the time evolution of mean values of meteorological variable fields we have calculated spectral distribution of their time series by using Fast Fourier Transform algorithm. Figure 12 shows an example of such distribution for the time series of geopotential height, temperature and kinetic energy averaged over all integration domain. One can see that the GM and RM spectras have a high degree of similarity. The high frequency tails quasi coincide. The year and semi-year oscillations have the same amplitude. Four year cycle in geopotential height and temperature is reproduced by RM and GM quasi identically. This cycle in kinetic energy spectra is also reproduced by both models but not identically. Also the models agree in reproducing of 6-9 years minimum and of the next increase of the spectra. Quasi all synoptic and seasonal oscillation maximums coincide in the RM and GM spectras. We calculated the same spectras for above mentioned regions shown in Figure 1. The RM and GM spectras for these regions demonstrate similar coincidence as that for all integration domain with insignificant distinctions. Only for the Pantanal region, the spectras of GM and RM kinetic energy at 1000 mb diverge significantly. But with the increase of altitude this difference diminishes and quasi disappears at 500 mb.

4. Conclusions

This analysis of the output results of 30-year runs of regional model and its driving global model confirms that the models have a high degree of consistency despite of the difference in their physical parameterizations. Therefore the described here version of the Eta model (INPE ETA CCS) driven by boundary conditions of HadAM3P can be used for the research applying the dynamical downscaling method. In the future work we are planning to estimate an impact of tuning in RM physical parameterizations such as radiation and convection schemes on consistency of RM and GM output fields. An impact of the use of another driven global model on the RM and GM resemblance will be also estimated. We also need to evaluate the model performance for current climate by comparing regional model outputs with observations. In order to estimate the impact of global model errors on the regional model outputs, the integration of the regional model driven by Reanalysis data is planned. The approach developed in this paper can form the basis for quantitative assessment of regional model and its driving global model consistency. Currently, many researchers use various regional models for dynamical downscaling but a few publications exist about the quantitative assessment of the similarity between the large-scale fields of a regional model and its driving global model. Even if regional and global models have the same physical parameterization packages, the difference between the models can be related to the low time frequency and low space resolution of boundary forcing in the regional model.

Acknowledgments. I.A. Pisnichenko was supported by Global Opportunity Fund (GOF) from UK Foreign Commonwealth Office, T.A. Tarasova was sponsored by INPE/CPTEC as part of an international agreement with the NEC Corporation. The authors thank their colleagues from CPTEC/INPE C. Nobre and J. Marengo for their administrative contributions that made it possible for us to perform this work. The authors also thank Hadley Center for presenting HadAM3P data.

References

Betts, A. K., and M. T. Miller, 1986: A new convective adjustment scheme. Part II: Single column tests GATE wave, BOMEX, and Arctic air-mass data. *Quart. J. Roy. Meteor. Soc.*, **112**, 693-703.

Black, T. L., 1994: NMC notes: the new NMC mesoscale Eta model: description and forecast examples. *Wea. Forecasting*, **9**, 256-278.

Chou, M.-D., and M. J. Suarez, 1999: A solar radiation parameterization (CLIRAD-SW) for atmospheric studies. Preprint, NASA/Goddard Space Flight Center, Greenbelt, Maryland, 38 pp.

Chou, M.-D.; Suarez, M.J., X.-Z. Liang, and M. M.-H. Yan, 2001: A thermal infrared radiation parameterization for atmospheric Studies. Preprint, NASA/Goddard Space Flight Center, Greenbelt, Maryland, 55 pp.

Chen F. K., Z. Janjic, and K. Mitchel, 1997: Impact of the atmospheric surface-layer parameterizations in the new land-surface scheme of the NCEP mesoscale Eta model. *Bound.-Layer Meteor.*, **85**, 391-421.

Christensen, J.H., T. Carter, and F. Giorgi, 2002: PRUDENCE employs new methods to assess European climate change.*EOS, Trans. Amer. Geophys. Union*, **82**, 147.

Chou, S.C., A.M.B. Nunes, and I.F.A. Cavalcanti, 2000: Extended forecastd over South America using the regional Eta model, *J. Geophys. Res.*, **105**, 10,147-10,160.

Chou, S.C., C.A.S. Tanajura, Y. Xue, and C.A. Nobre, 2002: Validation of the coupled Eta/SSiB model over South America. *J. Geophys. Res.*, **107**, 8088, doi:10.1029/2000JD000270.

Duffy, P.B., R.W. Arritt, J. Coquard, W Gutowski, J. Han, J. Iorio, J. Kim, L.-R. Leung, J. Roads, E. Zeledon, 2006: Simulations of present and future climates in the western United States with four nested regional climate models. J. Climate, 19, 873-895.

Dickinson, R.E., R.M. Errico, F. Giorgi, and G.T. Bates, 1989: A regional climate model for the western United States. *J.Climatic Change*, **15**, 383-422.

Fels, S. B., and M. D. Schwartzkopf, 1975: The simplified exchange approximation: A new method for radiative transfer calculations. *J. Atmos. Sci.*, **32**, 1475-1466.

Fernandez, J.P.R., S.H. Franchito, and V.B. Rao, 2006: Simulation of the summer circulation over South America by two regional climate models. Part I: Mean climatology. Theor. *Appl. Climatol.*, 86, 247-260.

Giorgi, F., X. Bi, J.S. Pal, 2004: Mean, interannual variability and trends in a regional climate change experiment over Europe. I. Present-day climate (1961-1990). Climate Dynamics, 22, 733-756, DOI 10.1007/s00382-004-0409-x.

de Gonsalves, L.G.G., W.J. Shuttleworth, S.C. Chou, Y. Xue, P.R. Houser, D.L. Toll, J. Marengo, and M. Rodell, Impact of different initial soil moisture fields on Eta model weather forecast for South America. *J. Geophys. Res.*, **111**, D17102, doi:10.1029/2005JD006309.

Hong, S.-Y., H.-M. Yuang, and Q. Zhao, 1998: Implementing of prognostic cloud scheme for a regional spectral model. *Mon. Wea. Rev.*, **126**, 2621-2639.

Janjic Z. I., 1994: The step-mountain eta coordinate model: further development of the convection, viscous sublayer, and turbulence closure schemes. *Mon. Wea. Rev.*, **122**, 927-945.

Jones R.G., J.M. Murphy, M. Noguer, A.B. Keen, Simulation of climate change over Europe using a nested regional-climate model. II: Comparison of driving and regional model responses t a doubling of carbon dioxide. *Q. J. R. Meteorol. Soc.*, **123**, 265-292.

Jones, R.G., M. Noguer, D.C. Hassel, D. Hudson, S.S. Wilson, G.J. Jenkins, and J.F.B. Mitchell, 2004: Generating high resolution climate change scenarios using PRECIS, Met. Office Hadley Center, Exeter, UK, 40 pp.

Kanamitsu, M., W. Ebisuzaki, J. Woollen, S.-K. Yang, J. J. Hnilo, M. Fiorino, and G. L. Potter, 2002: NCEP-DOE AMIP-II Reanalysis (R-2). *Bull. Amer. Meteor. Soc.*, **83**, 1631-1643.

Kain, J.S., and J.M. Fritsch, 1993: A one-dimensional entraining detraining plume model and its applications in convective parameterization.*J. Atmos. Sci.*, **23**, 2784-2802.

Lacis, A.A., and J.E. Hansen, 1974: A parameterization for the absorption of solar radiation in the Earth's atmosphere. *J. Atmos. Sci.*, **31**, 118-133.

Laprise, R., D. Caya, A. Frigon, D. Paquin, Current and perturbed climate as simulated by the second-generation Canadian Regional Climate Model (CRCM-II) over northwestern North America. *Climate Dynamics*, **21**, 405-421, DOI 10.1007/s00382-003-0342-4.

Mellor, G. L., and T. Yamada, 1974: A hierarchy of turbulence closure models for boundary layers. *J. Atmos. Sci.*, **31**, 1791-1806.

Mesinger F., Z.I. Janjic, S. Nickovic, D. Gavrilov, and D.G. Deaven, 1988: The step-mountain coordinate: model description and performance for cases of Alpine lee cyclogenesis and for a case of Appalachian redevelopment.*Mon. Wea. Rev.*, **116**, 1493-1518.

Misra, V., P.A. Dirmeyer, and B. Kirtman, 2003: Dynamical downscaling of seasonal simulations over South America. *J. Climate*, **16**, 103-117.

Nobre, P., A.D. Moura, and L. Sun, 2002: Dynamical downscaling of seasonal climate prediction over Nordeste Brazil with ECHAM3 and NCEP's Regional Spectral Models at IRI. *Bull. Amer. Meteor. Soc.*, **82**, 2787-2796.

Pisnichenko, I.A., T.A. Tarasova, J.P.R. Fernandez, and J. Marengo, 2006: Validation of the Eta WS regional climate model driven by boundary conditions from the HADAM3H over South America. Proceedings of 8 ICSHMO, Foz do Iguacu, Brazil, April 24-28, INPE, 595-597.

Roads, J., S. Chen, S. Cocke, L. Druyan, M. Fulakeza, T. LaRow, P.Lonergan, J.-H. Qian, and S. Zebiak, 2003: International Research Institute/Applied Research Centers (IRI/ARCs) regional model intercomparison over South America. *J. Geophys. Res.*, **108** (D14), 4425, doi:10.1029/2002JD003201.

Sun L., D.F.Moncunill, H.Li, A.D.Moura, F.A.S Filho, 2005: Climate downscaling over Nordeste, Btasil using the NCEP RSM97. *J. Climate*, **18**, 551-567.

Slingo, J. M., 1987: The development of a cloud prediction model for the ECMWF model, Quart. *J. Roy. Meteor. Soc.*, **113**, 899-927.

Tanajura, C.A.S., 1996: Modeling and analysis of the South American summer climate, Ph.D. thesis, 164 pp., Univ. of Md., College Park.

Tarasova, T. A., and B. A. Fomin, 2000: Solar radiation absorption due to water vapor: Advanced broadband parameterizations. *J. Appl. Meteor.*, **39**, 1947-1951.

Tarasova, T.A., J.P.R. Fernandez, I.A. Pisnichenko, J.A. Marengo, J.C. Ceballos, and M.J. Bottino, 2006: Impact of new solar radiation parameterization in the Eta Model on the simulation of summer climate over South America. *J. Appl. Meteor. Climatol.*, **44**, 318-333.

Xu, K.-M., and D. A. Randall, 1996: A semi empirical cloudiness parameterization for use in climate models. *J. Atmos. Sci.*, **53**, 3084-3102.

Figure captions

Figure 1. The regions over South America selected for the analysis: Amazonia (1), Nordeste (2), Sul Brasil (3), Minas (4), Pantanal (5).

Figure 2. Mean (1961-1990) fields of geopotential height (m), temperature (°K), and kinetic energy ($m^2 \sec^{-2}$) at 1000 mb, provided by HadAM3P (left) and Eta CCS model (right) simulations.

Figure 3. The same as in Figure 2 but at 700 mb.

Figure 4. Mean (1961-1990) dispersion fields of geopotential height (m), temperature (°K), and kinetic energy ($m^2 \sec^{-2}$) at 1000 mb, provided by HadAM3P (left) and Eta CCS model (right) simulations.

Figure 5. Mean (1961-1990) fields of bias (left), calculated from HadAM3P and Eta CCS model fields of geopotential height (m), temperature (°K), and kinetic energy ($m^2 \sec^{-2}$) at 1000 mb, and consistency index between HadAM3P and Eta CCS model(right), calculated for the same fields.

Figure 6. Definition of consistency index by using the coefficients of linear regression of HadAM3P field on Eta CCS model field.

Figure 7. Time series of mean (over the integration domain) bias and root mean square errors, calculated from HadAM3P and Eta CCS model fields of geopotential height (m), temperature (°K), and kinetic energy ($m^2 \sec^{-2}$) at 1000 mb (left) and 500 mb (right).

Figure 8. Time series of mean (over the regions shown in Figure 1) bias, calculated from HadAM3P and Eta CCS model fields of geopotential height, G (m), temperature, T (°K), and kinetic energy, KE ($m^2 \sec^{-2}$) at 1000 mb.

Figure 9. The same as in Figure 8 but at 700 mb.

Figure 10. Scattering diagram of daily coefficients (a0, a1) of linear regression of HadAM3P

field on Eta CCS model field of geopotential height at 1000 mb (top); time series of mean (over the integration domain) coefficients (a0, a1) (middle), time series of mean (over the integration domain) consistency index (bottom).

Figure 11. The same as in Figure 10 but for temperature at 1000 mb.

Figure 12. Time spectra of mean (over the integration domain) geopotential height (top), temperature (middle), and kinetic energy (bottom) at 1000 mb, provided by HadAM3P (solid) and Eta CCS model (dot-dashed) simulations.

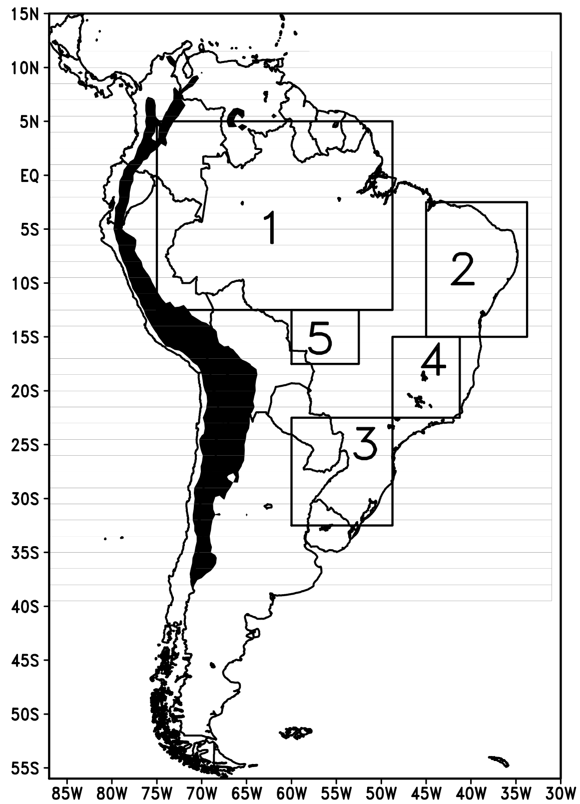

Figure 1: The regions over South America selected for the analysis: Amazonia (1), Nordeste (2), Sul Brasil (3), Minas (4), Pantanal (5).

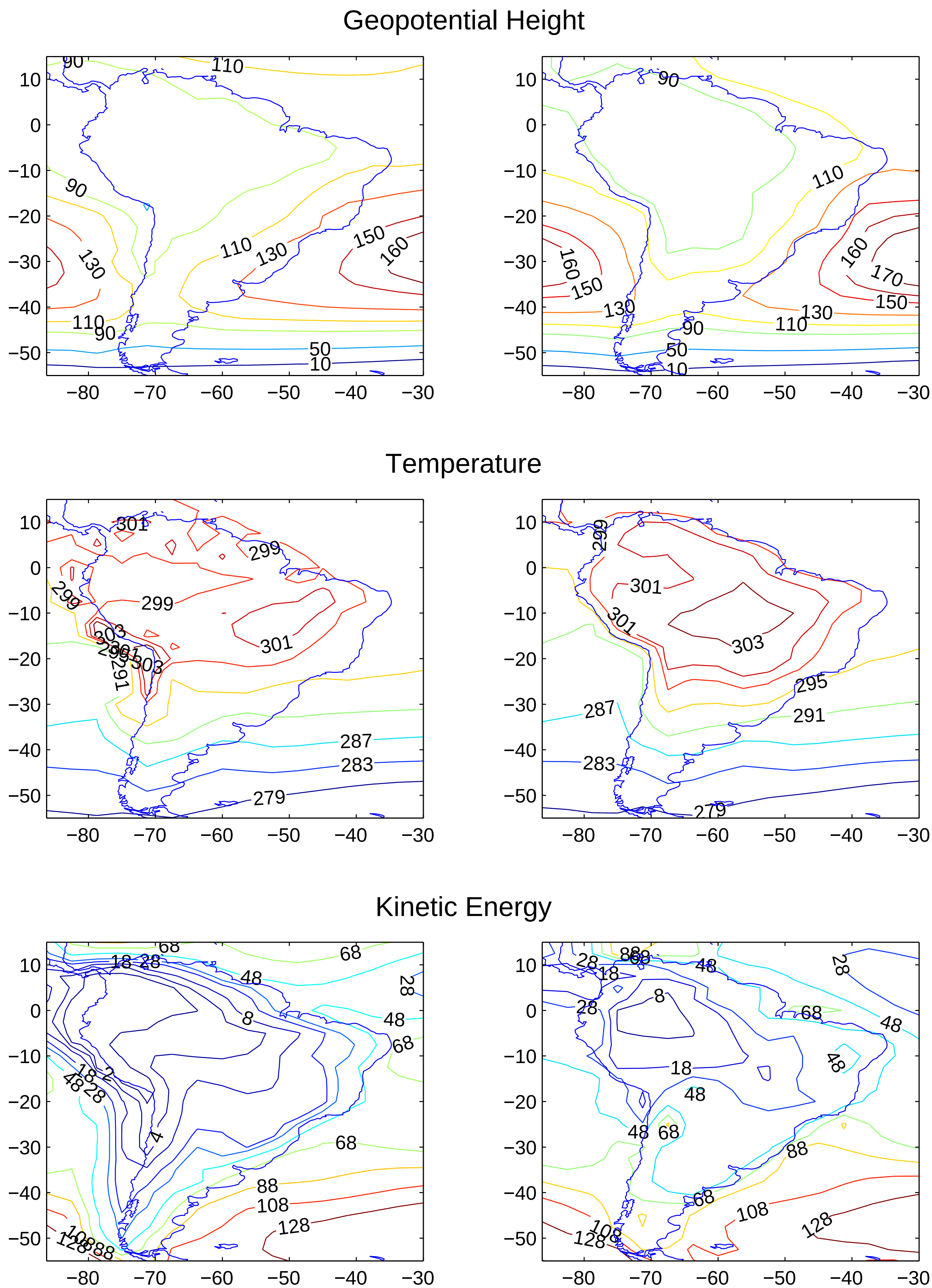

Figure 2: Mean (1961-1990) fields of geopotential height(m), temperature (°K), and kinetic energy ($m^2 \, sec^{-2}$) at 1000 mb, provided by HadAM3P (left) and Eta CCS model (right) simulations.

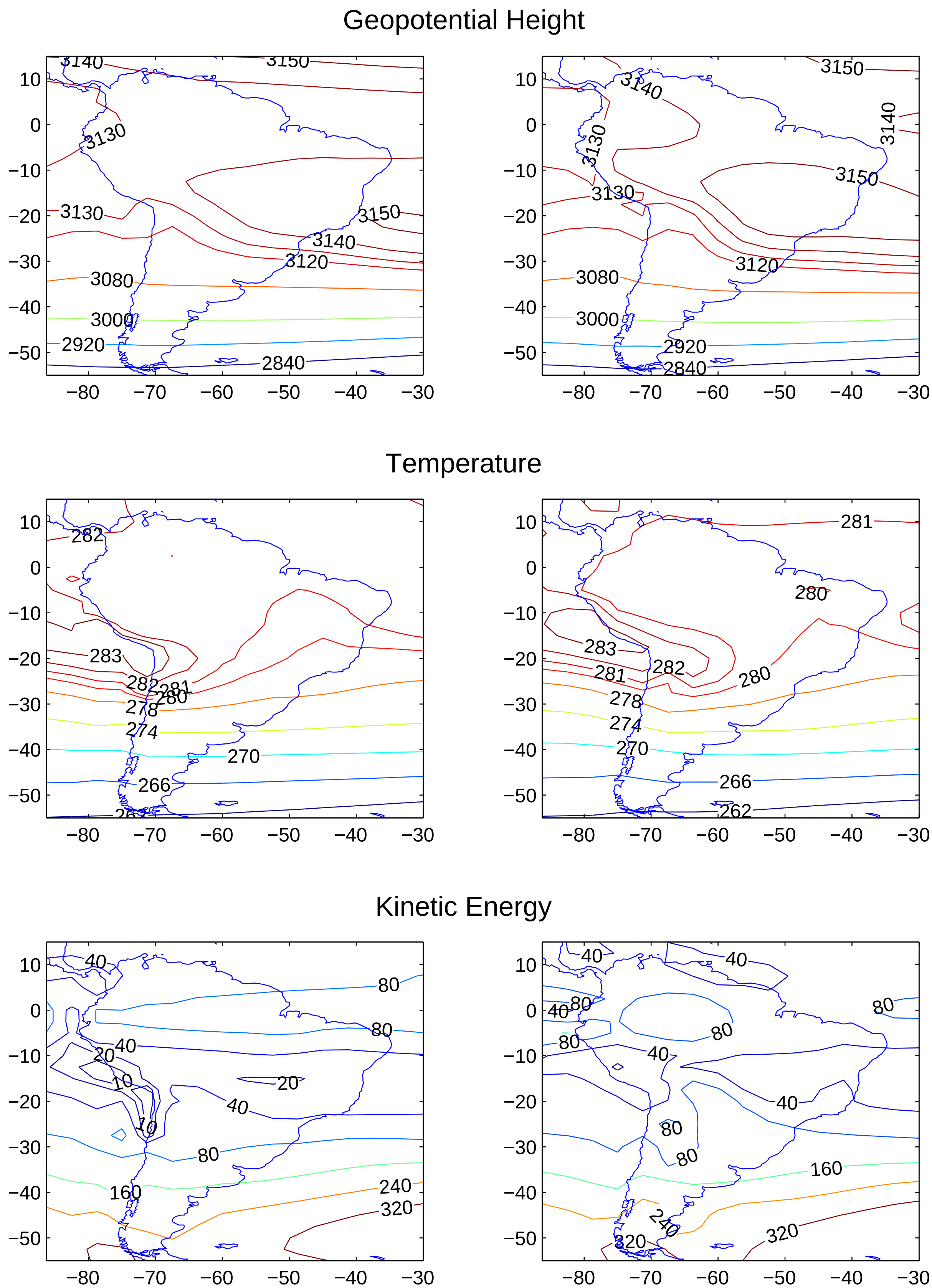

Figure 3: The same as in Figure 2 but at 700 mb.

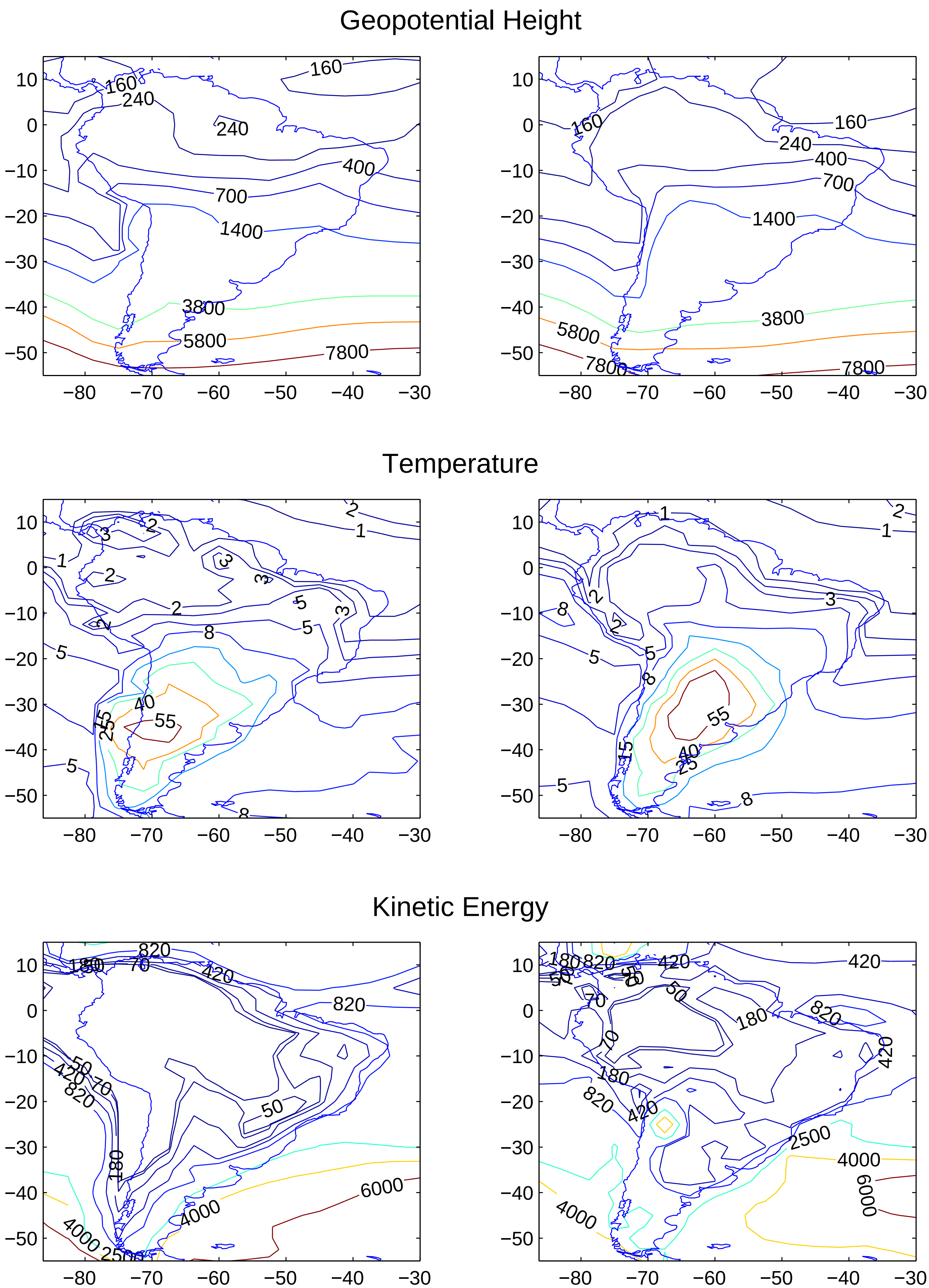

Figure 4: Mean (1961-1990) dispersion fields of geopotential height (m), temperature (°K), and kinetic energy ($m^2\ sec^{-2}$) at 1000 mb, provided by HadAM3P (left) and Eta CCS model (right) simulations.

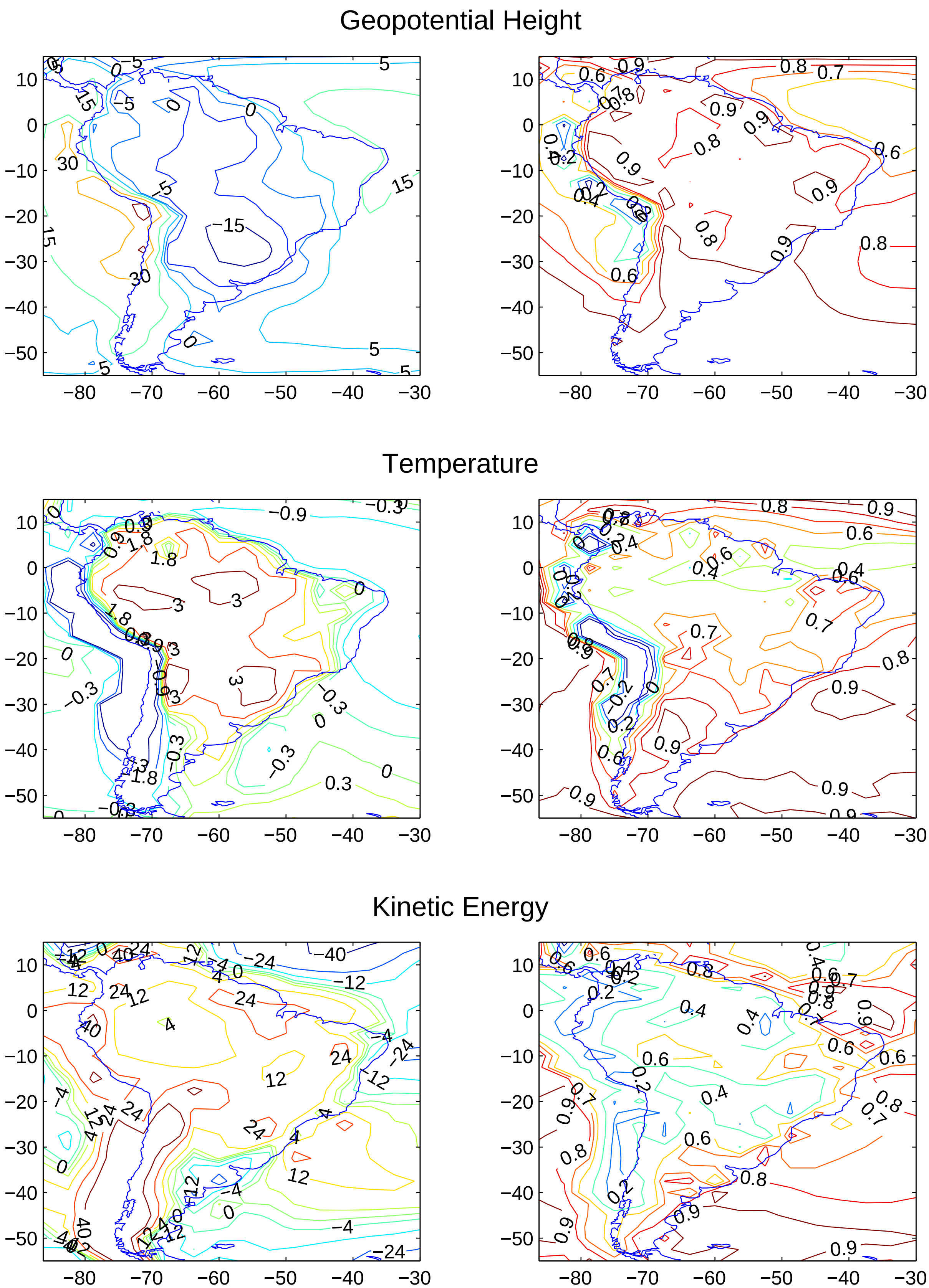

Figure 5: Mean (1961-1990) fields of bias (left), calculated from HadAM3P and Eta CCS model fields of geopotential height (m), temperature (°K), and kinetic energy ($m^2\ sec^{-2}$) at 1000 mb, and consistency index between HadAM3P and Eta CCS model(right), calculated for the same fields.

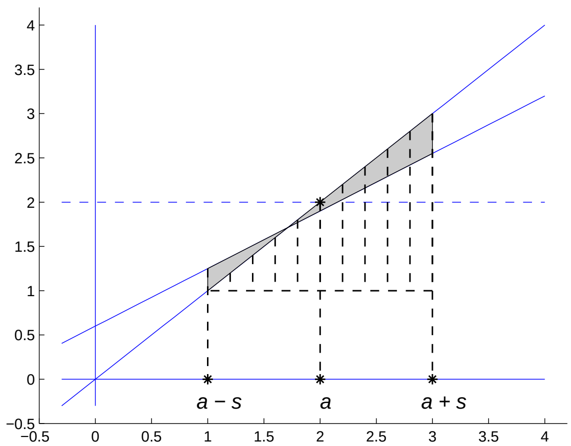

Figure 6: Definition of consistency index by using the coefficients of linear regression of HadAM3P field on Eta CCS model field.

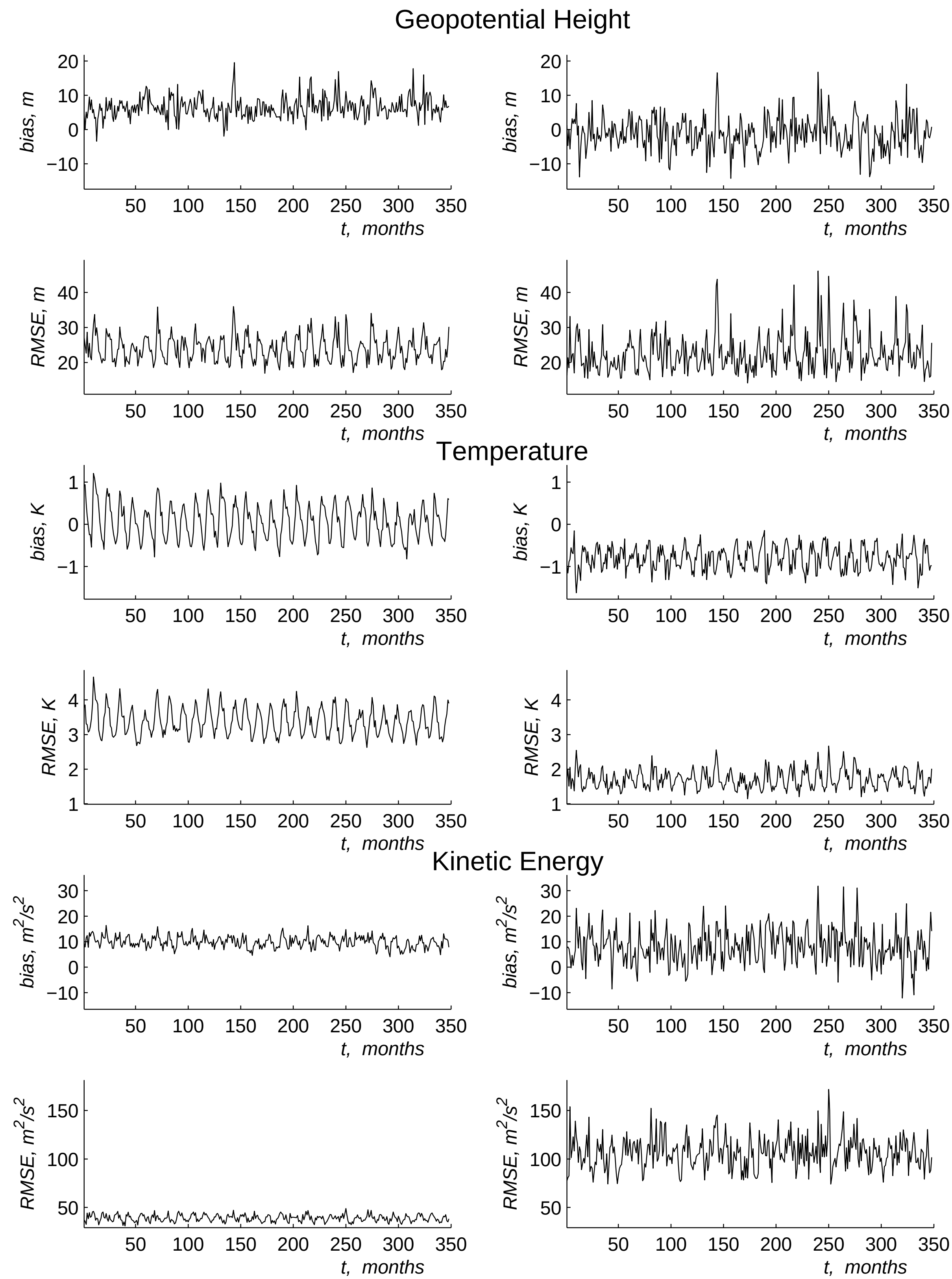

Figure 7: Time series of mean (over the integration domain) bias and root mean square errors, calculated from HadAM3P and Eta CCS model fields of geopotential height (m), temperature (°K), and kinetic energy ($m^2\,sec^{-2}$) at 1000 mb (left) and 500 mb (right).

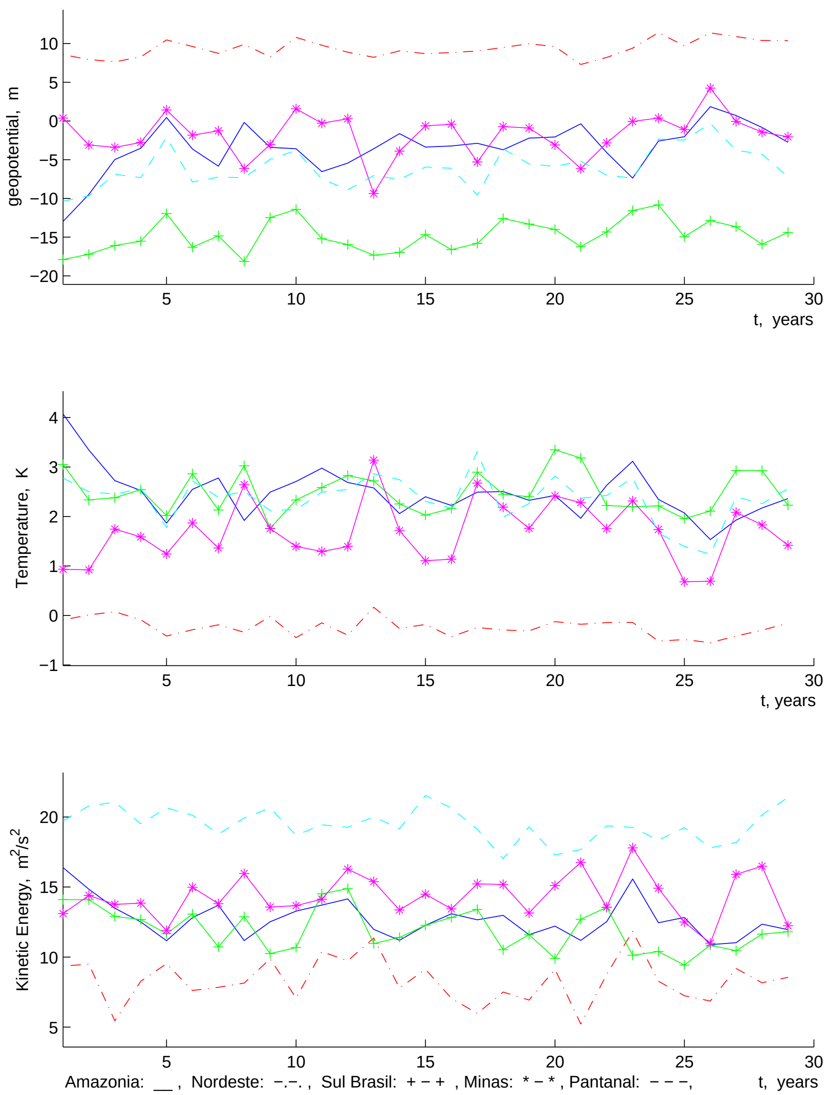

Figure 8: Time series of mean (over the regions shown in Figure 1) bias, calculated from HadAM3P and Eta CCS model fields of geopotential height, G (m), temperature, T (°K), and kinetic energy, KE ($m^2\ sec^{-2}$) at 1000 mb.

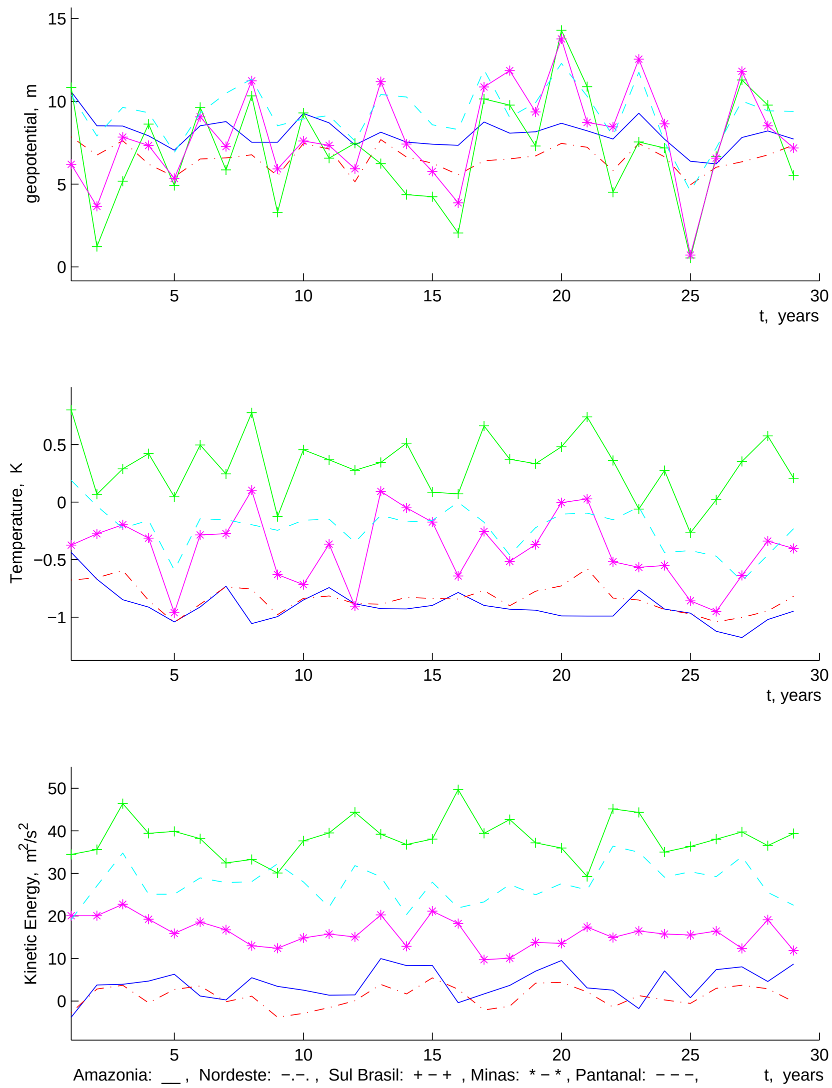

Figure 9: The same as in Figure 8 but at 700 mb.

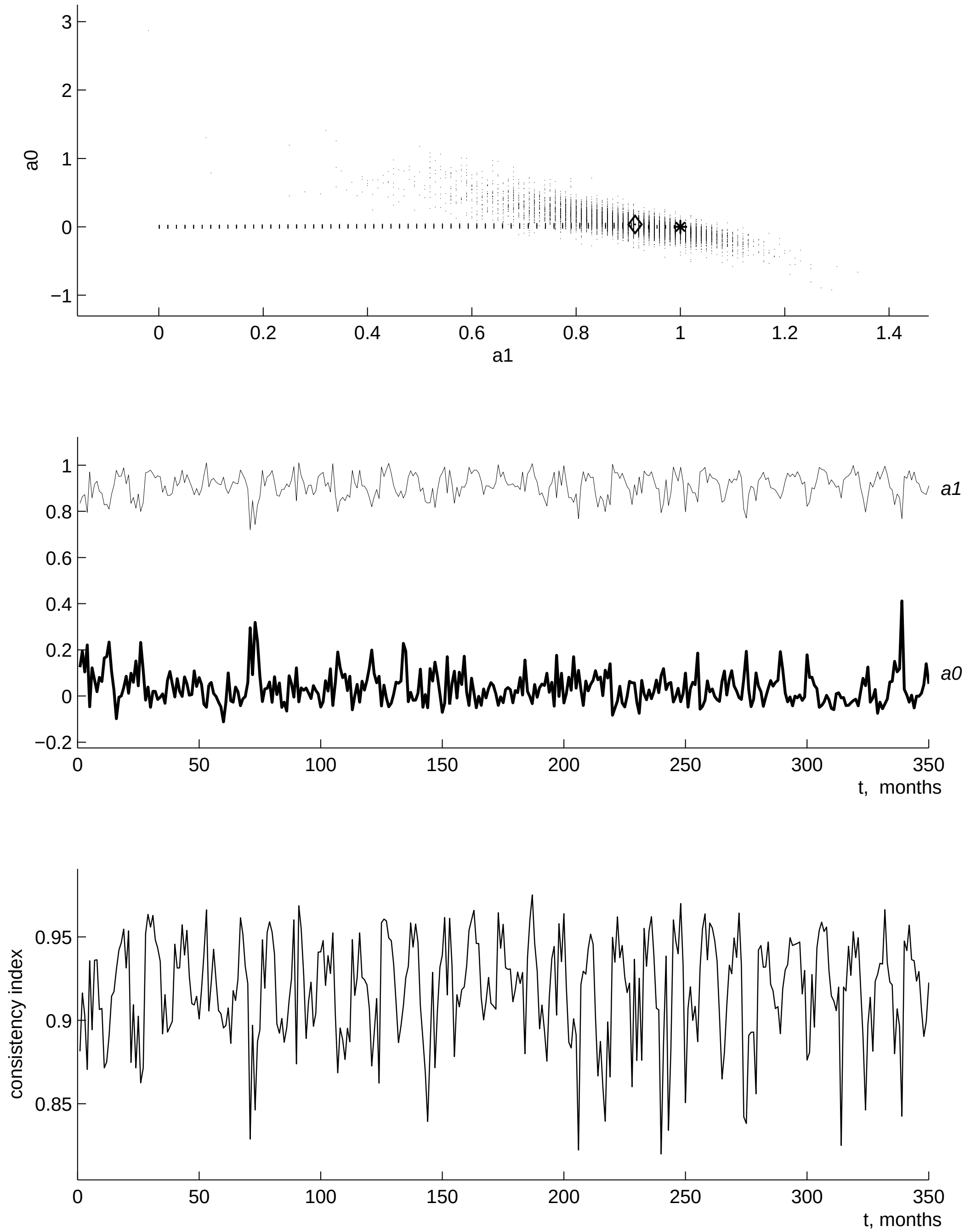

Figure 10: Scattering diagram of daily coefficients (a0, a1) of linear regression of HadAM3P field on Eta CCS model field of geopotential height at 1000 mb (top); time series of mean (over the integration domain) coefficients (a0, a1) (middle), time series of mean (over the integration domain) consistency index (bottom).

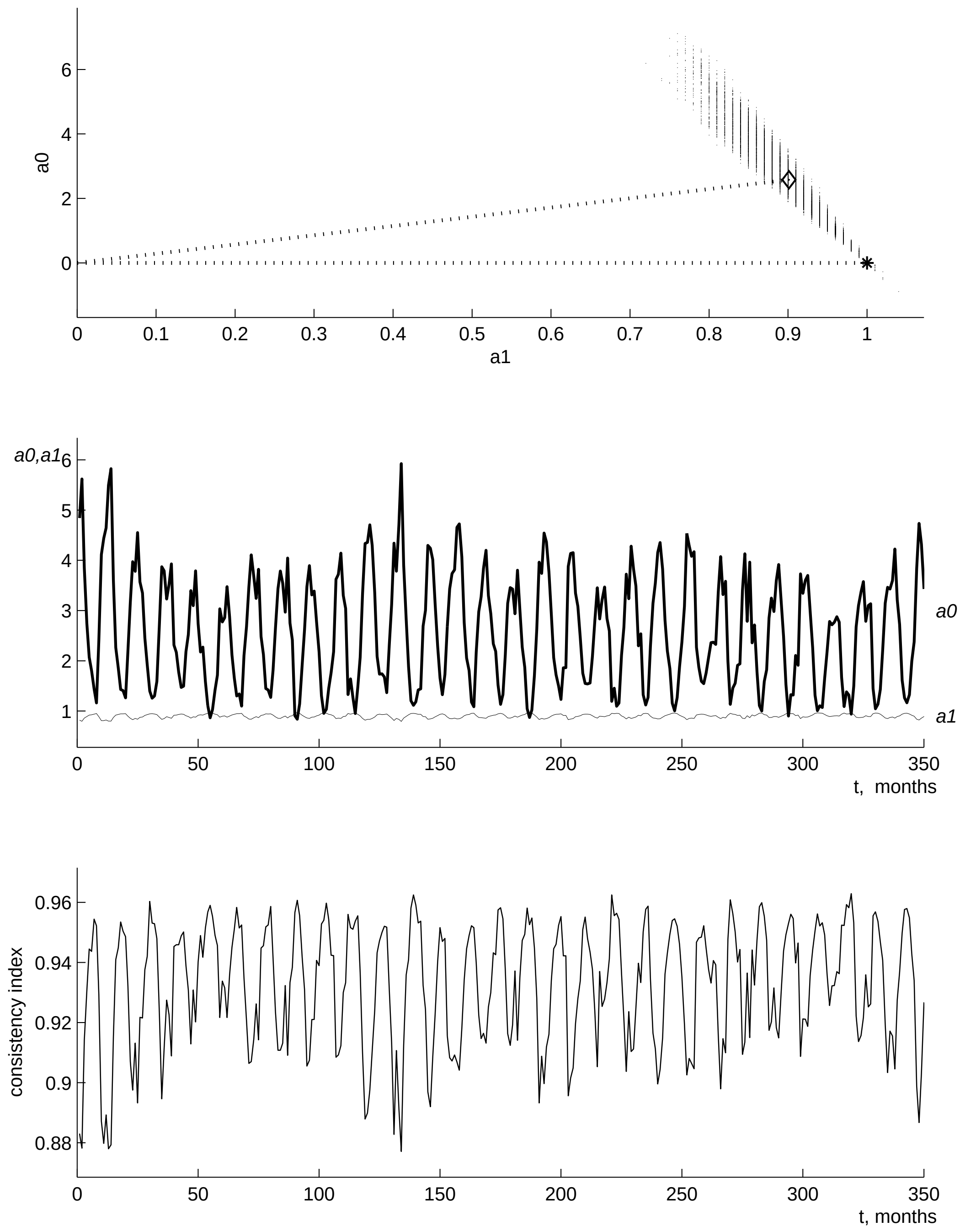

Figure 11: The same as in Figure 10 but for temperature at 1000 mb.

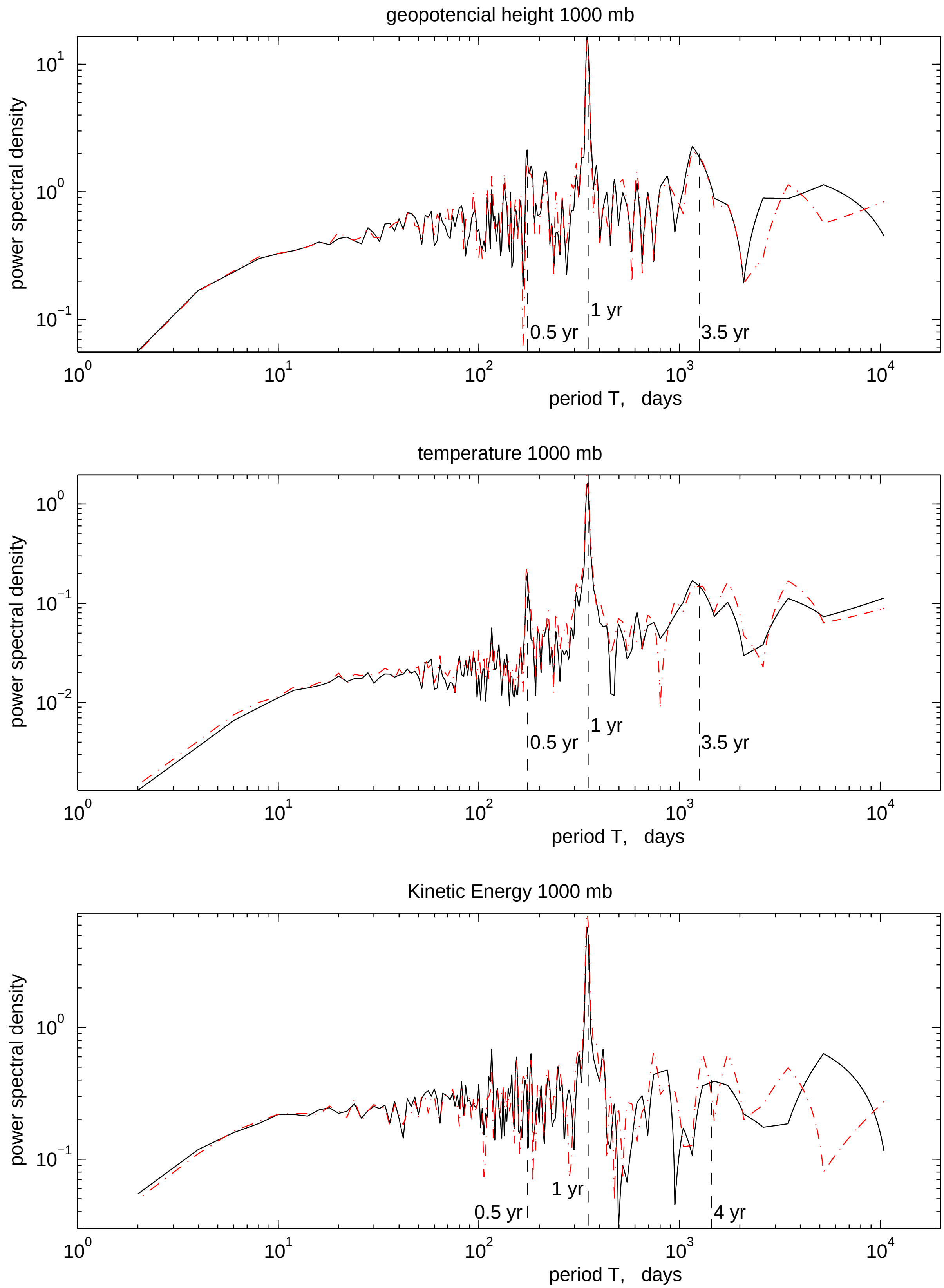

Figure 12: Time spectra of mean (over the integration domain) geopotential height (top), temperature(middle), and kinetic energy (bottom) at 1000 mb, provided by HadAM3P (solid) and Eta CCS model (dot-dashed) simulations.

Table 1. Mean correlation coefficient (r), mean bias , and mean RMS errors between the regional and global models time series of geopotential height (G), temperature (T), and kinetic energy (KE) at 1000 mb and 500 mb, averaged over the integration domain (D) and over the 5 regions shown in Figure 1.

	G			T			KE		
Region	r	Bias	RMSE	r	Bias	RMSE	r	Bias	RMSE
Pressure level of 1000 mb									
D	0.98	6	24	0.98	0.1	3.4	0.95	10	39
1	0.95	-3	9	0.78	2.5	3.0	0.51	13	17
2	0.97	9	13	0.92	-0.2	1.7	0.9	8	23
3	0.97	-15	25	0.96	2.5	4.2	0.83	12	27
4	0.95	-2	17	0.72	1.7	3.0	0.69	14	20
5	0.97	-6	14	0.64	2.4	3.5	0.79	20	22
Pressure level of 500 mb									
D	0.97	-1	23	0.99	-0.8	1.7	0.98	8	11
1	0.97	-2	6	0.81	-1.0	1.4	0.81	13	42
2	0.94	-1	8	0.81	-0.9	1.5	0.61	12	40
3	0.89	3	26	0.97	-1.0	1.8	0.93	7	111
4	0.74	2	16	0.88	-1.1	1.6	0.86	9	55
5	0.77	-1	10	0.79	-1.6	1.8	0.84	11	36